Available online at www.sciencedirect.com
SCIENCE DIRECT®
International Journal of Heat and Fluid Flow 26 (2005) 635–655
International Journal of HEAT AND FLUID FLOW
www.elsevier.com/locate/ijhff

Efficiency improvements of electromagnetic flow control

E. Spong, J.A. Reizes *, E. Leonardi

School of Mechanical and Manufacturing Engineering, The University of New South Wales, Sydney 2052, Australia

Accepted 1 April 2005
Available online 14 June 2005

Abstract

In turbulent flow, frictional resistance and heat transfer are controlled to a large degree by the intensity of the turbulence fluctuations in the near vicinity of a surface. In the case of a weak electrically conducting fluid, such as seawater, turbulence intensity can be controlled by subjecting the fluid to electromagnetic fields. This technique, known as Electro-magneto-hydro-dynamic (EMHD) flow control, has been shown to have promise as a means of reducing the turbulence intensity, and hence heat transfer or frictional drag of turbulent boundary layers. Unfortunately EMHD flow control currently suffers from poor efficiency due to the high energy requirements of the electromagnetic field.

A numerical study has been conducted in which a new electromagnetic actuator design has been developed to provide a more efficient spatial distribution of the electromagnetic forces. The new actuator design has then been coupled to an *ideal* flow sensor. A flow control subroutine, embedded in the numerical model, uses the velocity information from the *ideal* sensor to determine the appropriate actuating force to apply to the flow at each time step.

The new actuator design has been shown to be capable of successfully attenuating a sequence of artificial low speed streaks in a simplified model of a low Reynolds number turbulent boundary layer. Thus, a potential solution to the poor efficiency of EMHD flow control has been offered by providing the means whereby the expensive electromagnetic forces can be strategically and sparingly applied to the flow.

Keywords: Turbulence control; Near-wall turbulence; Electro-MHD actuators; Lorentz forces; Flow sensors

1. Introduction

Electro-magneto-hydro-dynamic (EMHD) flow control offers a possible means of reducing and enhancing the intensity of the turbulence fluctuations in the near vicinity of a surface and therefore a means of influencing the heat transfer from a surface to a surrounding fluid. In such applications the electromagnetically generated force field, or Lorentz field as it is more commonly known, is generated by arrays of magnets and electrodes, called actuators, placed just beneath or on a wall.

Traditionally two types of actuator design have been used. One type generates a Lorentz field which is mostly parallel to the wall in the streamwise direction (Henoch and Stace, 1995; Crawford and Karniadakis, 1997) and the other generates a Lorentz field. which is mostly normal to the wall (Du et al., 1998). Although actuators which generate forces normal to the wall show promise of successfully controlling turbulent fluctuations (Du and Karniadakis, 2000), this paper will focus on efficiency improvements to the first mentioned design, hereafter referred to as a streamwise actuator.

In the case of streamwise actuators, attempts have been made to reduce turbulence intensity by accelerating the near-wall, $y^+ < 20$, flow thereby inhibiting the formation of low speed streaks (Henoch and Stace, 1995). Low speed streaks are known to be precursors to the turbulence inducing an '*ejection-burst-sweep*' process so that a decrease in the number of low speed

* Corresponding author. Fax: +61 2 9663 1222.
E-mail address: reizes@cfd.mech.unsw.edu.au (J.A. Reizes).

0142-727X/$ - see front matter © 2005 Elsevier Inc. All rights reserved.
doi:10.1016/j.ijheatfluidflow.2005.04.001

steaks would reduce the turbulence intensity of the near wall flow.

EMHD flow control possesses many advantages as a method of boundary layer control chief among these being that it is capable of producing a time dependent force with a response time many orders of magnitude faster than the smallest timescales of turbulent boundary layer flows. In addition to this it is not confined to the wall but is a true three-dimensional force capable of penetrating deep into the boundary layer. Unfortunately, EMHD flow control currently suffers from a low efficiency as a result of two significant disadvantages.

2. Deficiencies of existing streamwise actuator designs

Firstly, traditional streamwise actuator designs are incapable of accelerating the near wall flow ($10 < y^+ < 20$) without themselves inducing large friction forces at the wall ($y^+ = 0$) (Henoch and Stace, 1995; Crawford and Karniadakis, 1997; Du et al., 1998) hence enhancing turbulence intensity contrary to the intended strategy.

Traditional streamwise actuators designs are composed of long slender magnets and electrodes mounted immediately beneath the wall, each with its axis aligned in the streamwise direction. The spanwise positioning of the magnets and electrodes is that they alternate as magnet, electrode, magnet, electrode and so on. In addition both magnets and electrodes are arranged with alternating polarities.

A typical example of this configuration, utilizing three magnets and three electrodes, is shown in cross-section in Fig. 1. The interaction of the magnetic field $\boldsymbol{B}$ and electric field $\boldsymbol{E}$ (dark and light vectors respectively) is also shown. For clarity the vectors are all shown at uniform lengths. The magnetic and electric fields are essentially two dimensional in the spanwise/wallnormal plane of Fig. 1 with very little variation in the streamwise direction due to the long slender nature of the magnets and electrodes. The magnetic field was modeled by applying a current across the magnet surfaces and using the Biot-Savart Law to compute the resulting $\boldsymbol{B}$ field. Similarly the electric field was modeled by applying a charge density to the electrode surfaces and using Coulomb's Law to compute the resulting $\boldsymbol{E}$ field (Spong, 2003).

Close inspection of Fig. 1 reveals the root cause of the design deficiency. Note that many of the magnetic and electric vectors immediately adjacent to the wall ($y^+ < 5$) are aligned at or close to 90° to one and another. As may be seen in Eq. (1) the magnitude of the Lorentz force $\boldsymbol{L}$ is, in part, a function of the angle of orientation φ between the electric $\boldsymbol{E}$ and magnetic $\boldsymbol{B}$ fields and that for φ equal to 90° the Lorentz force will be at its maximum.

$$|\boldsymbol{L}| = |\boldsymbol{J} \times \boldsymbol{B}| = \sigma |\boldsymbol{E}||\boldsymbol{B}| \sin \varphi \tag{1}$$

In addition to this the $\boldsymbol{B}$ and $\boldsymbol{E}$ fields are strongest near the wall and each decays at a rate proportional to the square of the distance above the wall so that the Lorentz forces will decay approximately as the 4^{th} power of the distance from the wall. The combination of these two facts, the 90° alignment between the $\boldsymbol{B}$ and $\boldsymbol{E}$ fields and the natural wallnormal decay in each field, means that the Lorentz forces immediately adjacent to the wall ($y^+ < 5$) are substantially higher than those further away. The wallnormal decay in the Lorentz force is clearly visible in Fig. 2. Calculations

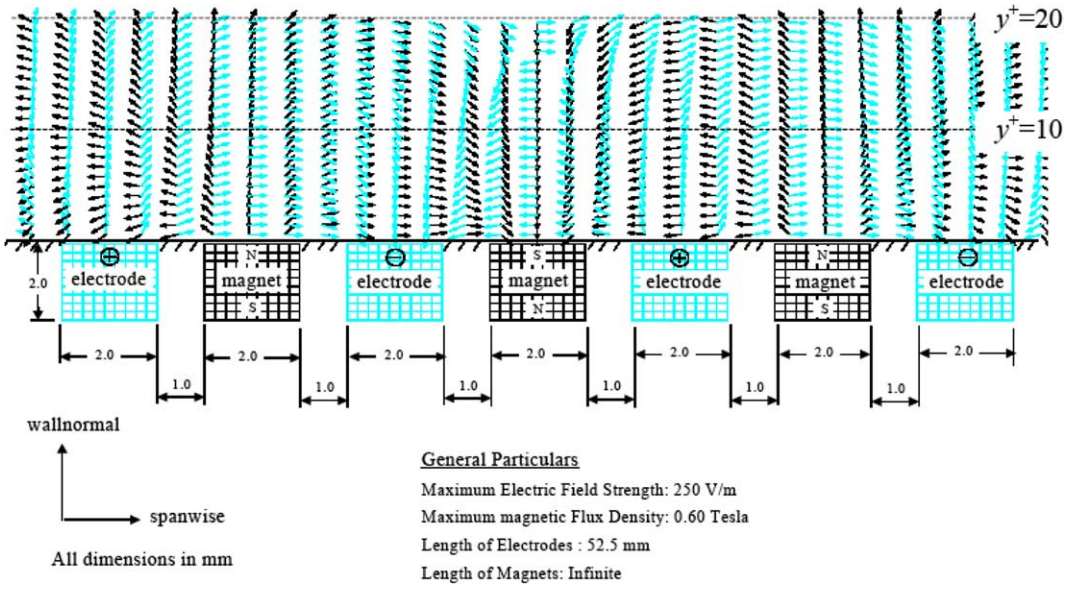

Fig. 1. Cross-section of a typical EMHD actuator showing interaction of magnetic and electric fields.

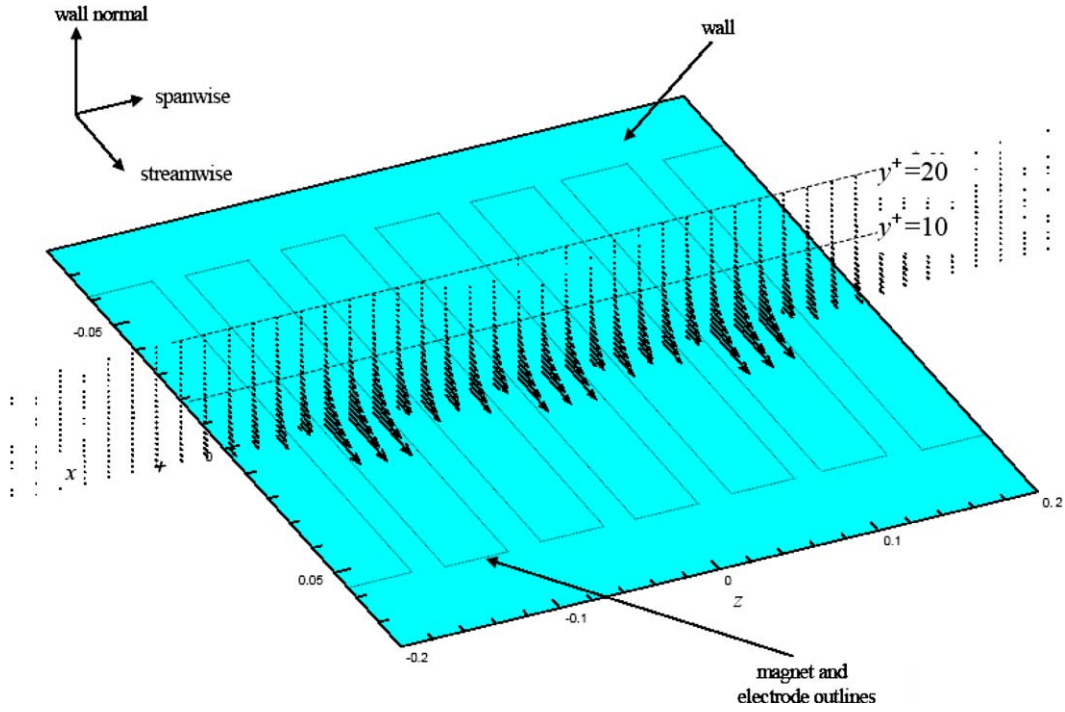

Fig. 2. Cross-sectional view of the Lorentz field $\boldsymbol{L}$ of the EMHD actuator shown in Fig. 1, using a fluid electrical conductivity of 4.5 Si/m.

performed in the present study show that the Lorentz forces at $y^+ = 5$, $y^+ = 10$ and $y^+ = 15$ are on average equal to 21%, 3.6% and 0.3% of the Lorentz forces at $y^+ = 0$ respectively. This may be seen in Fig. 3.

Of concern is the fact that any form of control in the $10 < y^+ < 15$ region, where the low speed streaks are to be found, can not be accomplished without introducing large near wall ($y^+ < 5$) Lorentz forces. These forces will have the immediate and direct effect of increasing the frictional drag and turbulence intensity at the wall. Clearly this is one of the major factors responsible for the poor efficiency of EMHD flow control for turbulence reduction. The strong decay in the Lorentz force wallnormal profile must therefore be altered if any improvement in the ability, and indeed efficiency, of the actuator to control the low speed streaks is to be achieved.

3. A new EMHD actuator

Given that both the magnetic and electric fields decay at a rate proportional to the square of the distance from their respective sources it may be seen from Eq. (1) that

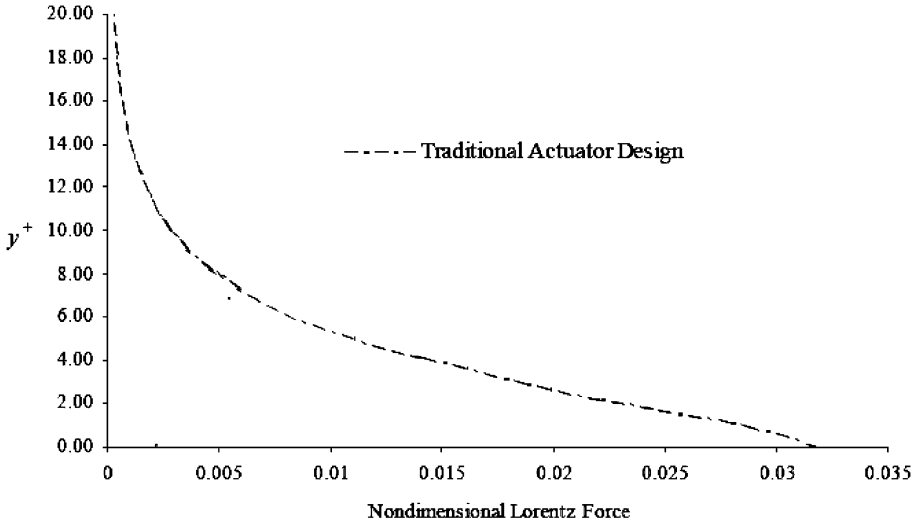

Fig. 3. Wallnormal profile of $\boldsymbol{L}$ for the actuator of Fig. 1. Values non-dimensionalised by 675 N/m^3.

the Lorentz field, taken purely as a function of the two field strengths and ignoring any variation in the angles between the two fields, can be expected to decay proportionally to the fourth power of the distance from its source. However, the decay may be attenuated, even reversed, if the electric and magnetic fields can be carefully re-orientated with respect to one and another. It is this re-orientation of the electric and magnetic fields that is the fundamental principle on which the design philosophy for the new EMHD actuator has been founded.

Eq. (1) indicates that when the magnetic and electric field vectors are aligned at 90° to each other the local Lorentz force will be at its maximum. When the magnetic and electric field vectors are aligned at either 0° or 180° to each other the local Lorentz force will be zero. The strategy is then to align the electric and magnetic fields parallel to each other near the wall ($y^+ < 5$) and align them at close to 90° in the $10 < y^+ < 15$ region where the low speed streaks are expected. This is the optimal alignment.

With this strategy in mind, the question then arises as to which features of the actuator can best be used to manipulate the alignment between the electric and magnetic vectors. Only three design options have been investigated in past EMHD studies. These are to vary the strength (Crawford and Karniadakis, 1997), the spanwise spacing (Du et al., 1998) and the cross-sectional area (Du et al., 1998) of the magnets and electrodes.

While individually these options are not without merit, collectively they provide a rather limited scope for design, especially in the context of the design strategy to be undertaken in the present study. Thus, there is a strong need to expand the 'design space' of EMHD actuators and to develop new and innovative options to increase the extent of design possibilities.

The present authors have taken up this challenge, the results of which may be seen in the actuator design of Fig. 4. One way of expanding the 'design space' of EMHD actuators is to focus efforts on introducing options aimed at enhancing the ability to manipulate the shape of the magnetic field. To date the magnets used in actuator designs have invariably been placed immediately adjacent to the wall. That is, the upper surface of the magnets is located at $y^+ = 0$ so that they are in contact with the fluid. While it is essential that the electrodes be in contact with the fluid in order to transmit current through the fluid there is no need for the magnets to be in contact with the fluid. Unlike the electric currents, the magnetic fields can readily be transmitted through free space. On this basis the magnets may be moved away from the wall, as may be seen in Fig. 4, thereby significantly increasing the flexibility of the design.

The design space may also be considerably expanded by introducing magnets of different relative strengths. This is in contrast to existing actuator designs which have invariably employed magnets of equal strength (Berger et al., 2000; Posdziech and Grundmann, 2001). For the actuator design shown in Fig. 4 the two south magnets (upper face is the south pole) have been set at

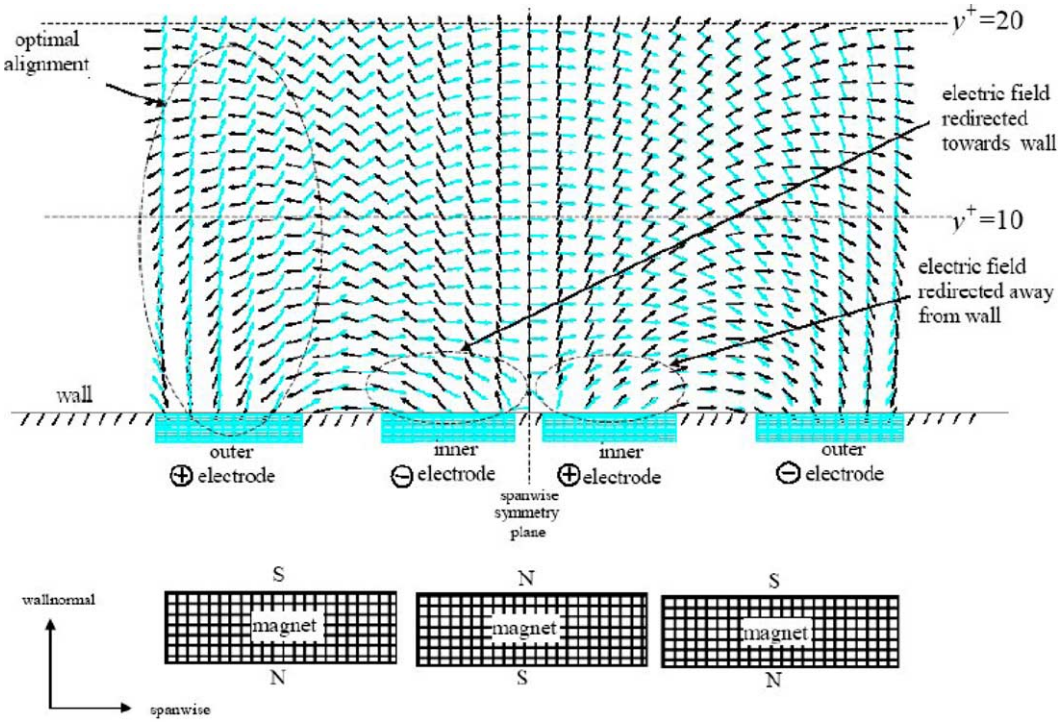

Fig. 4. New Actuator—preliminary design showing cross-sectional view of electric and magnetic fields.

40% of the strength of the north magnet (upper face is the north pole).

In addition to the measures focused on manipulating the magnetic field, options aimed at manipulating the electric field have also be explored in the design shown in Fig. 4. However, it should be noted that since the electrodes must remain in contact with the fluid the scope for expanding the 'design space' of the electrodes is somewhat more limited. Nonetheless an option that is readily available, and to date unexplored in previous EMHD studies, is the option of introducing electrodes of different voltages. For the actuator design shown in Fig. 4 the inner electrodes have been set at 30% of the voltage of the outer electrodes.

Although the design shown in Fig. 4 demonstrates much promise in reducing the wallnormal decay in the Lorentz field, particularly in the region above the outer electrodes, a facility for a far more precise alignment of the electric and magnetic fields is required if the decay is to be sufficiently attenuated for practical flow control applications.

From Eq. (1) it can be seen that the strength of the Lorentz force is linearly proportional to the sine of the angle between the electric and magnetic fields. However the sine of the angle is not linearly proportional to the angle itself. At angles near 0° and 180° the sensitivity of the sine function to small angle changes is at its maximum. That is the sine curve has its steepest gradient at 0° and 180° degrees and these are the electric/magnetic alignment angles being sought near the wall ($y^+ < 5$) in order to minimize the Lorentz force in this region. Thus, small misalignments between the electric and magnetic fields in this region will cause large changes in the Lorentz force. This effect is accentuated by the fact that the magnitudes of the electric and magnetic fields are large near the wall. In short there is only a small range of alignment angles that will adequately reduce the near wall ($y^+ < 5$) Lorentz forces to the point that they cease to dominate the Lorentz forces further away from the wall ($y^+ > 10$).

The requirement for a more precise field alignment may be realized by further expanding the design space of the actuator to include composite magnets and electrodes. Composite magnets and electrodes have not hitherto been used in the field of EMHD flow control.

It may be seen from Fig. 5 that the composite magnets and electrodes are obtained by partitioning the existing magnets and electrodes, shown in Fig. 4, into a number of smaller similar components. For example the positive outer electrode has been subdivided into a number of smaller adjacent positive electrodes and the north magnet has been subdivided into a number of smaller adjacent north magnets. A suitable insulation material is placed between each sub-component.

By varying the relative strengths of each of the smaller components a more localized, and hence more precise, control can be achieved over the magnetic and electric field alignments in the near wall region. Inspection of Fig. 5 shows that for almost the entire spanwise extent of the actuator the electric and magnetic vectors are aligned at close to either 0° or 180° in the $0 < y^+ < 5$ region and at close to 90° in the $10 < y^+ < 15$ region as per the intended design strategy.

The resultant Lorentz field may be seen in Fig. 6. Inspection of this Lorentz field shows that not only have

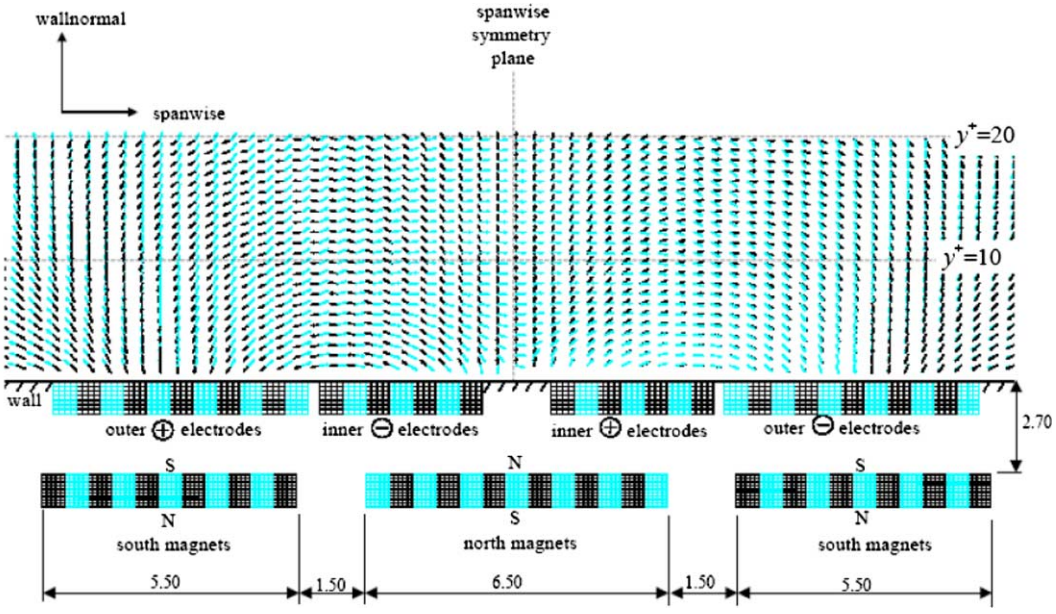

Fig. 5. New Actuator—final design showing cross-sectional view of electric and magnetic fields. Magnet and electrode dimensions in mm.

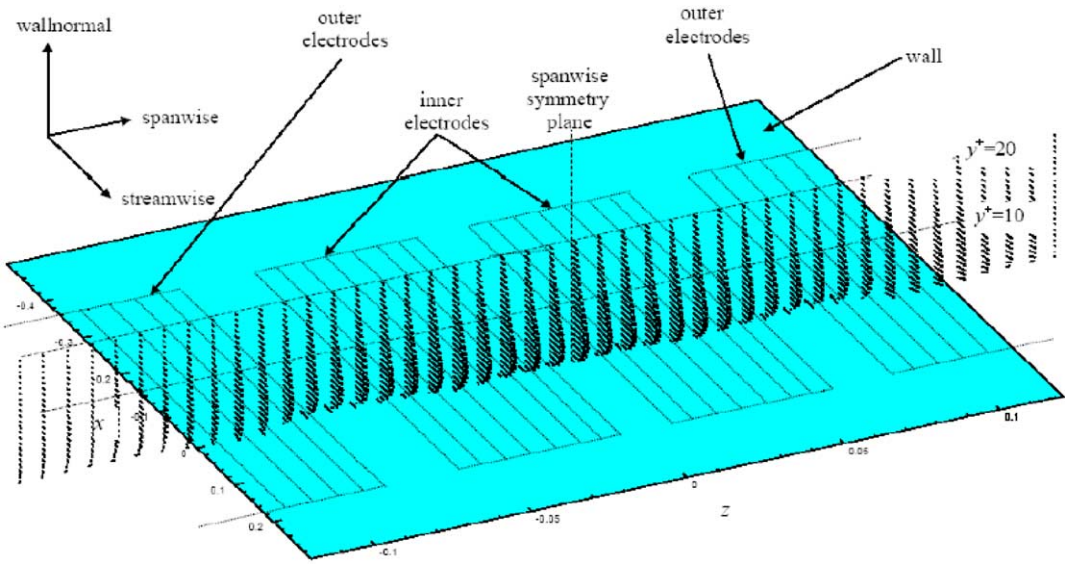

Fig. 6. Final Design Concept—cross-sectional view of Lorentz field.

the decaying wall normal profiles been attenuated but in fact parabolic wallnormal profiles have been induced for almost the entire spanwise extent of the actuator with the average height of the maximum Lorentz force in the parabolic profiles being approximately $y^+ = 5$. Although this height is below the target range of $10 < y^+ < 15$ the actuator configuration shown in Fig. 5 clearly constitutes a significant improvement in the design of EMHD actuators in that the issue of the wall normal decay in the strength of the Lorentz force field has been solved. This is clearly shown in Fig. 7 where the wall normal profiles of the traditional and new design are compared. Having produced an appropriate Lorentz force distribution it is now possible to examine various strategies for its operational control.

4. The new EMHD actuator coupled to an ideal sensor

The second significant disadvantage of EMHD flow control is that, to date, the actuators have either been permanently activated or the actuators have been pulsed at arbitrary frequencies. Regrettably, EMHD actuators have high power requirements, thus it is critical that the actuators be sparingly employed.

In addition, it is also important that EMHD actuators be strategically applied to the flow in order to reduce the instances of unnecessary and potentially counterproductive forces being used on the flow. Thus, there is a strong need to couple the EMHD actuators to some form of sensor so that the EMHD forces are applied only when and where they are required.

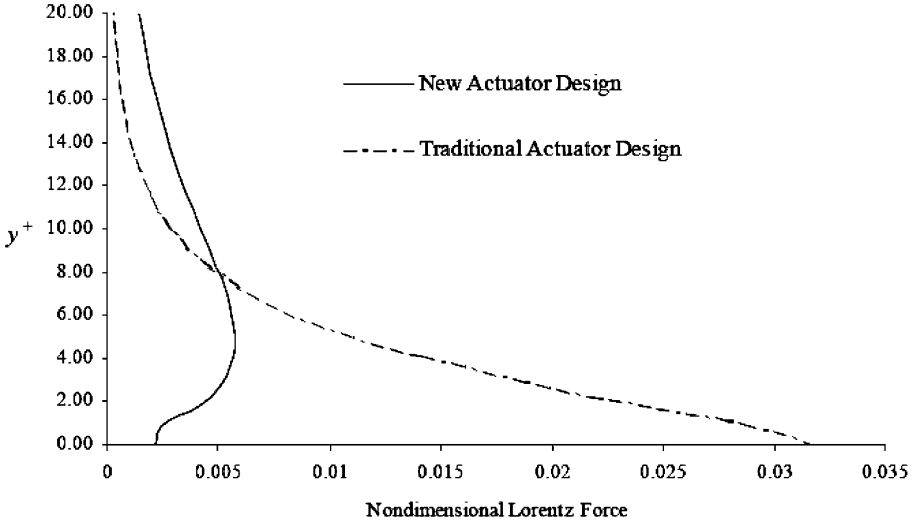

Fig. 7. Wallnormal profile of Lorentz Forces for the traditional actuator and the new actuator. Values non-dimensionalised by 675 N/m^3.

For the present study the new EMHD actuator design has been coupled to an *ideal* flow sensor which detects the presence of low speed streaks. The sensor is *ideal* in that it operates inside a numerical model of the flow where it directly accesses the fluctuations in streamwise velocity u' at $y^+ = 12$ immediately above the actuator (Spong, 2003). This may be seen in Fig. 8.

A flow control subroutine, embedded in the numerical model, determines the course of action the actuator should take based on the *ideal* sensor velocity information. The first task of the flow control subroutine is to identify the presence of any low speed streaks which have come into the vicinity of the actuator. Whilst a variety of methods are obviously available for processing the array of u' values obtained from the *ideal* sensor, for simplicity, it was decided in the present study to compute the spanwise average of the u' values and fit a cubic spline as may be seen in Fig. 8. A streamwise profile of the spanwise averaged u' values is therefore generated.

A search is then made along this streamwise profile for negative local minima. A negative local minimum is understood to signify the presence of a low speed streak. The position, magnitude and convective velocity of the local minimum is deemed to represent the position, magnitude and convective velocity of the low speed streak.

Following the search, one of four actions will then be taken. If no negative local minimum is located in the streamwise profile then it is assumed that there is no low speed streak over the actuator so that the Lorentz force field need not be activated. Likewise, if a negative local minimum is located but its magnitude is below a threshold value, for the present study this is 20% of the expected mean strength of low speed streaks, then the Lorentz force field is not activated. This facility allows the flow control subroutine to selectively target only those streamwise velocity fluctuations associated with the low speed streaks and to filter out the other smaller velocity fluctuations in the flow.

If a low speed streak is identified in the vicinity of the actuator then a series of checks are made to determine whether control should be initiated on the streak. It is important that the streak be allowed to convect a short distance over the actuator before control is initiated. This is to ensure that the Lorentz forces are not prematurely activated so as to not expend unnecessary energy on the streak before it is within range. A check is therefore made to see whether the streak has been convected over the required distance of the actuator as may be seen in Fig. 9. Investigations have shown that this distance should be approximately 15% of the actuator length L_{actuator}.

A check is also made to see whether the detected streak has not suddenly formed over the downstream extent of the actuator as shown by distance 'B' in Fig. 10. In contrast to a streak that forms upstream of the actuator and then is convected through the upstream boundary of the actuator, a streak that suddenly forms over the downstream extent of the actuator will not be in the vicinity of the actuator for a sufficient length of time to be effectively attenuated. Thus control will not be initiated on a low speed streak if it has not first passed through the upstream boundary of the actuator.

When a low speed streak has been identified over the actuator and, once the above checks have been passed, a sequence of target values for the associated negative minimum in the u' streamwise profile (see Fig. 8) is then generated. The sequence is constructed prior to initiating control of the streak and serves to map out the

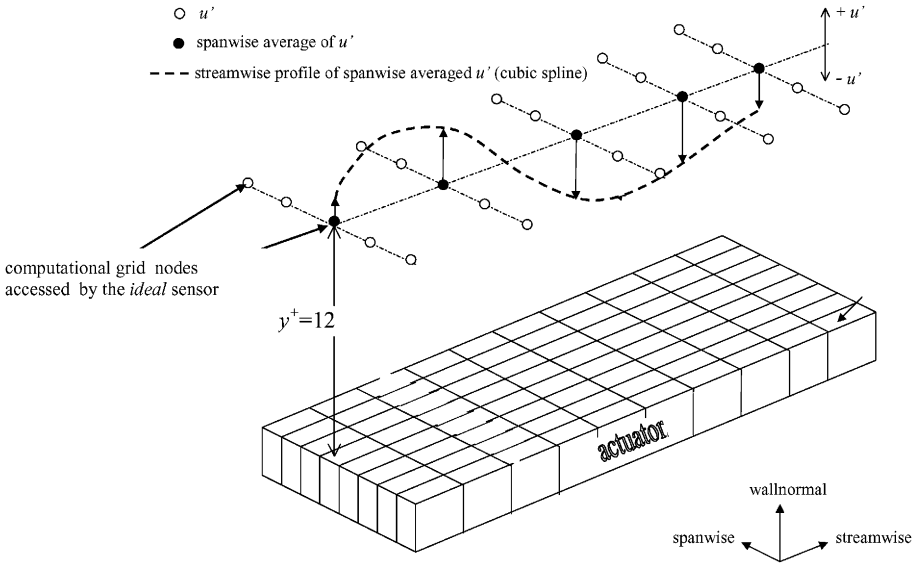

Fig. 8. *Ideal* flow sensor detecting the presence of streamwise velocity fluctuations u' over the actuator.

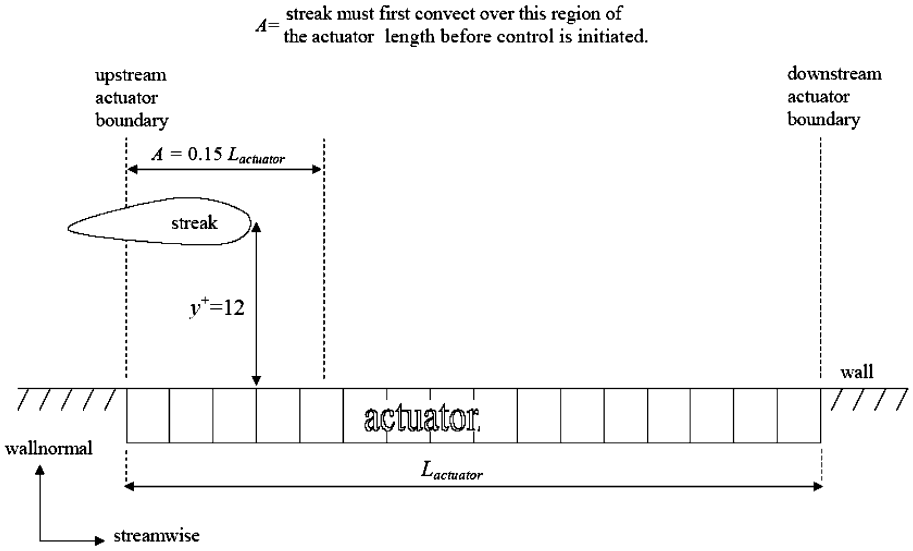

Fig. 9. A low speed streak must convect the distance 'A' over the actuator length before control is initiated.

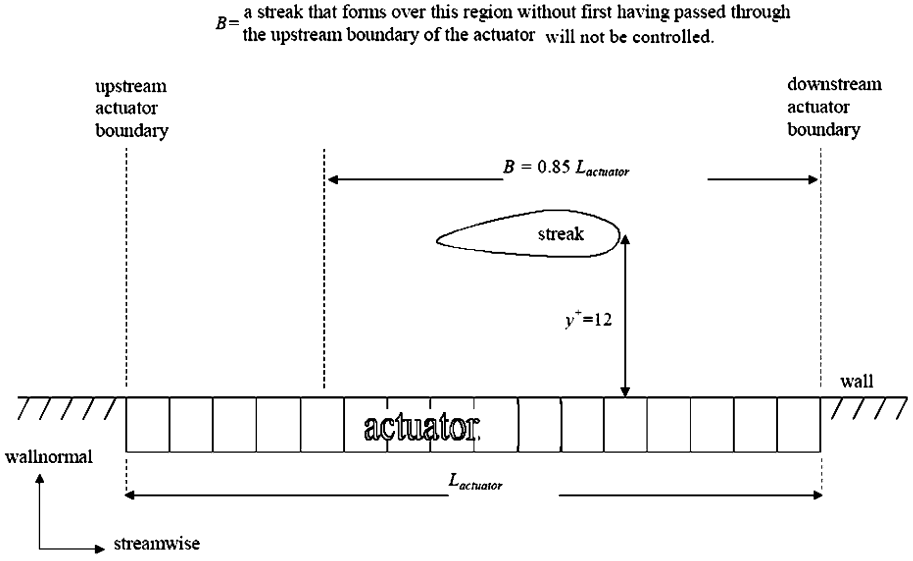

Fig. 10. Low speed streaks that form over the down stream extent of the actuator will not be controlled.

intended attenuation of the streak. A typical sequence of target values for a negative local minimum is shown in Fig. 11. The sequence is constructed by selecting a series of control points and fitting a cubic spline through the points.

To construct the sequence of target values initial and final values, shown as control points '0' and '2' respectively in Fig. 11, are selected. The initial value corresponds to the instantaneous magnitude of the local minimum and the final value corresponds to the desired magnitude of the local minimum as the streak leaves the vicinity of the actuator. For the present study the intention is to completely attenuate the streak by the time it leaves the vicinity of the actuator so the final target value will be zero.

An estimate of the length of time available in which to attenuate the streak, that is the length of time for which the streak will be in the vicinity of the actuator, must also be made. This length of time is referred to as the control interval as shown in Fig. 11. The length of the control interval is calculated as

$$t_{\text{control}} = \frac{0.85 L_{\text{actuator}}}{u_{\text{streak}}} \tag{2}$$

where u_{streak} is the convective velocity of the streak which is calculated as

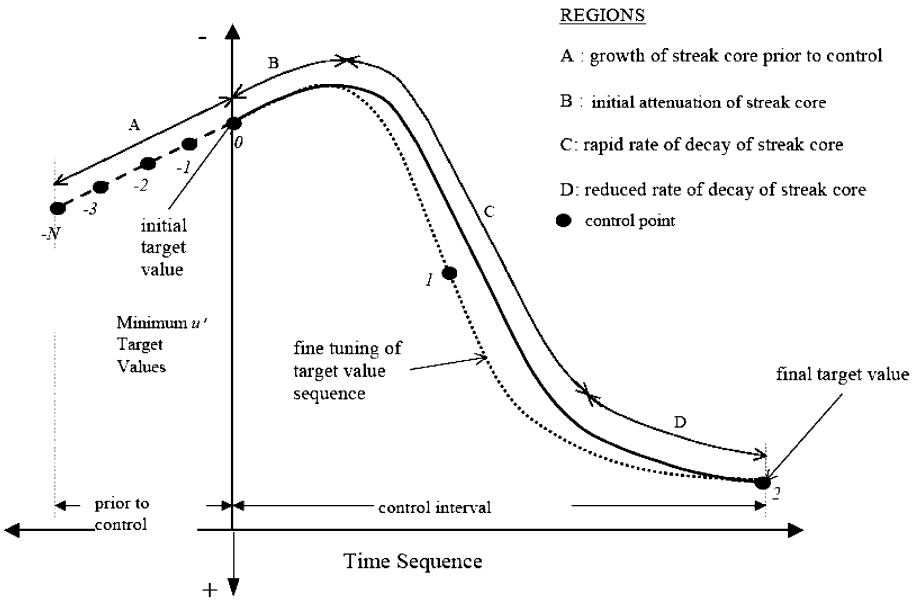

Fig. 11. A typical time sequence of target values for the minimum u' value representing a low speed streak.

$$u_{\text{streak}} = \frac{A}{t_A} \tag{3}$$

where A is the distance shown in Fig. 9 and t_A is the time taken for the streak to be convected the distance A. Once the control interval has been determined a sequence of intermediate target values is then generated over the control interval as shown in Fig. 11.

To ensure that the Lorentz forces vary smoothly in time the sequence of intermediate target values is constructed so that the control commences by seeking only a small rate of attenuation in the streak. Thus the initial portion of the target value sequence, shown as region B in Fig. 11, must take into account the uncontrolled or natural development of the streak just prior to the commencement of control, shown as region A. This is accomplished by including a series of N control points, shown as control points '-1' to '$-N$', which represent the magnitudes of the local minimum at the N timesteps immediately prior to the commencement of control. A value of $N = 20$ was found to sufficiently represent the natural development of the streak just prior to the commencement of control.

The remainder of the target value sequence is constructed so that, following the initially small rate of attenuation, the rate of attenuation is then progressively increased, shown as region C in Fig. 11, reaching a maximum near the middle of the control interval and then reduced over the final stages, shown as region D. Reducing the final stages of the attenuation in this fashion ensures that the streak does not leave the vicinity of the actuator with any excess energy from the Lorentz forcing. The rate of attenuation over regions C and D is fine tuned using control point '1' shown in Fig. 11. For the present study the vertical co-ordinate of control point '1' is given as

$$y_1 = 0.5(y_0 + y_2) \tag{4}$$

while the horizontal co-ordinate is given as

$$x_1 = 0.5(x_0 + x_2) \tag{5}$$

where (x_0, y_0) and (x_2, y_2) are the co-ordinates for control points '0' and '2' respectively.

Once the target value sequence has been constructed the progressive attenuation of the streak is then undertaken by seeking to drive the local minimum representing the streak to the appropriate target value at each time step of the control interval. To do this the flow control subroutine must compute the appropriate strength of Lorentz force to be generated by the actuator at each of the control interval time steps.

This is accomplished by predicting the responses of the instantaneous flow field to a range of different strength Lorentz fields and then selecting the Lorentz field strength which corresponds closest to the instantaneous local flow field being driven in the desired direction.

To predict the responses of the instantaneous flow field to a given Lorentz field strength in a computationally efficient manner a technique, based on a linear superposition of velocity fields, has been developed by the present authors. The linear superposition of velocity fields is given by

$$\underline{u}' + \Delta \underline{u}_{\text{nat}} + C\underline{u}_{\text{ind}} = \underline{u}^{t+\Delta t} \tag{6}$$

in which $\underline{u}^t$ is the instantaneous velocity field local to the actuator. $\underline{u}^t$ is obtained from the solution of the Navier–Stokes equations computed at the previous time step of

the flow simulation, $\underline{u}^{t+\Delta t}$ is the instantaneous velocity field which is estimated to result from the $\underline{u}^t$ field being driven in a particular direction over the time interval Δt. The $\underline{u}^{t+\Delta t}$ field will depend on a number of influences exerted over the $\underline{u}^t$ field including the influence of the applied Lorentz field. The aim then is to determine the required strength of the Lorentz field such that the $\underline{u}^{t+\Delta t}$ field closely matches the desired condition towards which we wish to drive the $\underline{u}^t$ field.

The above mentioned influences exerted over the $\underline{u}^t$ field are accounted for in the $\Delta\underline{u}_{\text{nat}}$ and $\Delta\underline{u}_{\text{ind}}$ velocity fields. In other words the magnitude and shape of the $\Delta\underline{u}_{\text{nat}}$ and $\Delta\ \underline{u}_{\text{ind}}$ velocity fields determines the resulting $\underline{u}^{t+\Delta t}$ velocity field.

The first of these fields, the $\Delta\underline{u}_{\text{nat}}$ field, is the change that would occur in $\underline{u}^t$ if the solution were progressed forward one time step interval Δt in the absence of any Lorentz forces being applied to the flow. It provides an estimate for the direction in which the $\underline{u}^t$ flow field would "naturally" develop if left uncontrolled over the time interval Δt. $\Delta\underline{u}_{\text{nat}}$ therefore accounts for the presence of the turbulent flow structures which need to be controlled in combination with the history of Lorentz forces that have been applied to these flow structures over the previous time steps. $\Delta\underline{u}_{\text{nat}}$ need only be computed once per time step by advancing the solution $\underline{u}^t$ one time step forward but with the Lorentz force terms set to zero.

The $\Delta\underline{u}_{\text{ind}}$ velocity field by contrast accounts exclusively for the Lorentz force field to be applied during the current time step. Whereas $\Delta\underline{u}_{\text{nat}}$ accounts for the component of change in $\underline{u}^t$ due to the natural or uncontrolled development of the flow, progressed forward over the time interval Δt, $\Delta\underline{u}_{\text{ind}}$ accounts for the component of change in $\underline{u}^t$ due to the controlled development of the flow induced by a given Lorentz force field. As such $\Delta\underline{u}_{\text{ind}}$ acts as the counter balance or corrector to the term $\Delta\underline{u}_{\text{nat}}$.

The $\Delta\underline{u}_{\text{ind}}$ field is linearly varied using the scaling factor C until the resulting $\underline{u}^{t+\Delta t}$ velocity field matches the desired condition towards which we wish to drive the $\underline{u}^t$ field. The Lorentz field strength associated with this match is then selected as being the required strength of the actuator for that time step.

5. Results

To demonstrate its performance a sequence of artificial low speed streaks, one of which may be seen in Fig. 12a, were run over the actuator. The control objective is to fully attenuate each streak before it departs through the downstream boundary of the actuator. The artificial low speed streaks were generated by applying a wallnormal velocity condition at the upper boundary of the computational domain, located at $y^+ = 20$, as shown in Fig. 12b. The wallnormal velocity condition replicates the interaction of the legs of a hairpin vortex on the viscous sublayer in a manner similar to that which gives birth to the low speed streaks in a real turbulent boundary layer. The artificial low speed streaks have been modeled to correspond with the $Re = 3300$ turbulent channel flow investigated numerically by Kim et al. (1987).

To assess the performance of the actuator shown in Fig. 5 the attenuation of a single artificial low speed streak is examined in detail. In addition to examining the performance of the new actuator design, the performance of an actuator employing the traditional electrode and magnet arrangement, shown in Fig. 1, is also investigated for the purposes of comparison.

Some noticeable differences between the performance of the new actuator design and the traditional actuator design may be seen when contour plots of the instantaneous u' values are taken in the $y^+ = 12$ plane. These are shown in Figs. 13–16. Figs. 13a, 14a, 15a and 16a constitute a time sequence for an uncontrolled artificial low speed streak. Figs. 13b, 14b, 15b and 16b constitute the time sequence for the same artificial low speed streak as controlled by the new actuator design, while the control of the artificial streak using the traditional actuator design may be seen in Figs. 13c, 14c, 15c and 16c.

The time sequence commences with the artificial low speed streak, indicated by the dark central contours, located 10% along the actuator length. Since the control of the streak has not commenced, it must be at least 15% along the length before control is initiated, Figs. 13a, 13b and 13c are identical. Note also the artificial high speed streaks, indicated by the dark contours, which can be clearly seen on either side of the low speed streak.

Shortly after the commencement of control a noticeable difference may be seen between the uncontrolled artificial streak shown in Fig. 14a and the artificial streak, shown in Fig. 14b, which is controlled by the new actuator design. The size and intensity of the artificial streak has been significantly attenuated as indicated by the smaller region of dark grey contours. It can be seen in Fig. 14c that the size and intensity of the artificial streak has also been reduced by the traditional actuator but at the expense of increasing the intensity of the high speed streaks.

A comparison of Fig. 15a and 15b then show that by the time the artificial streak is 65% of the way along the length of the actuator it has almost been entirely attenuated by the new actuator. Of equal note is the fact that this attenuation has been accomplished without the actuator unnecessarily introducing any strong positive fluctuations in the streamwise velocities. The same cannot be said for the traditional actuator. It may be seen in Fig. 15c that although the artificial low speed streak is almost entirely attenuated the artificial high speed

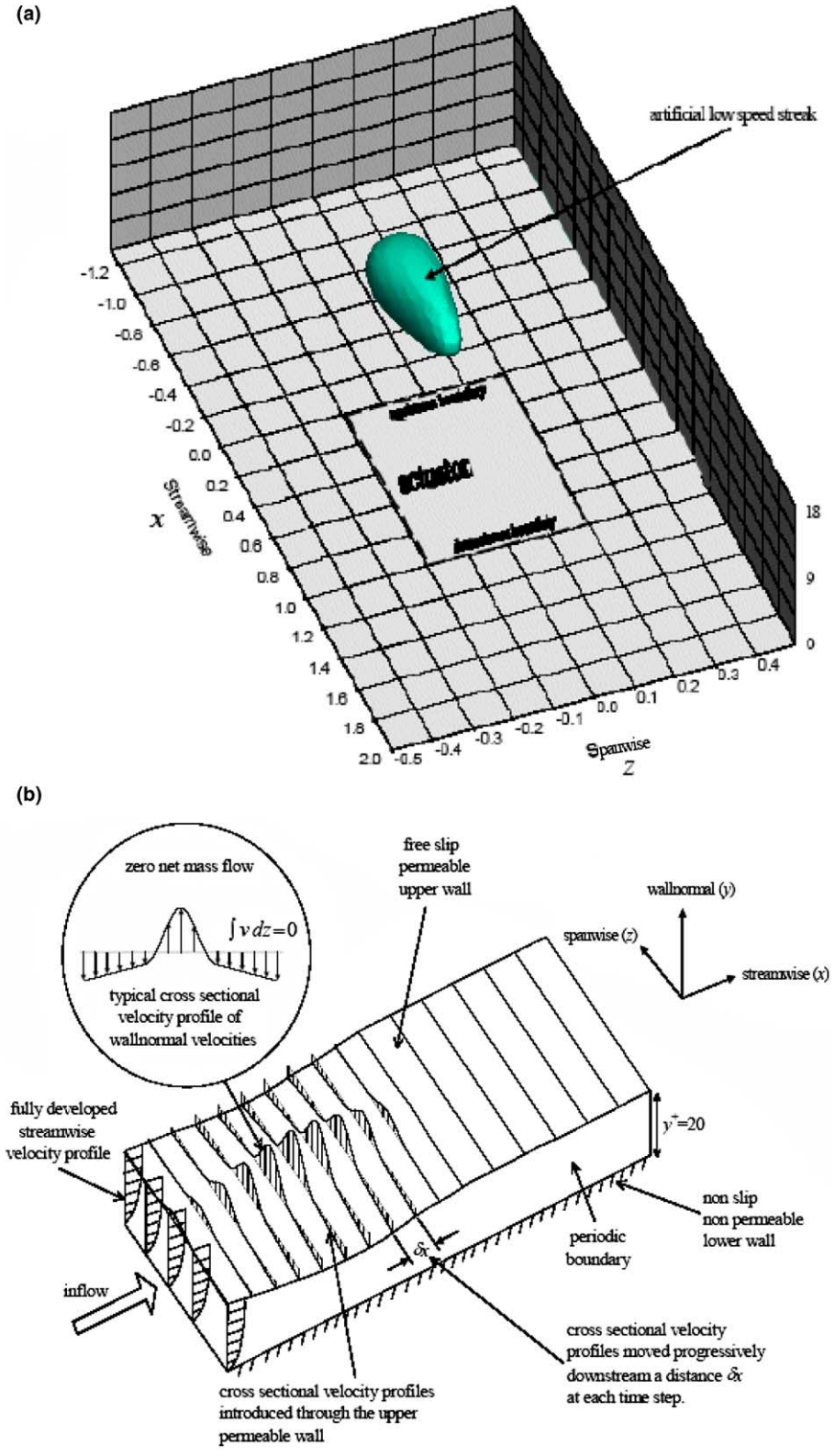

Fig. 12. (a) An artificial low speed streak shown as it convects over the actuator. Streamwise and spanwise dimensions are normalised by the actuator length. (b) Boundary conditions used to generate the artificial low speed streaks including the wallnormal velocity condition at the upper boundary.

streaks have intensified significantly in comparison with their uncontrolled state.

The fact that the new actuator has been able to attenuate the low speed streak without introducing any

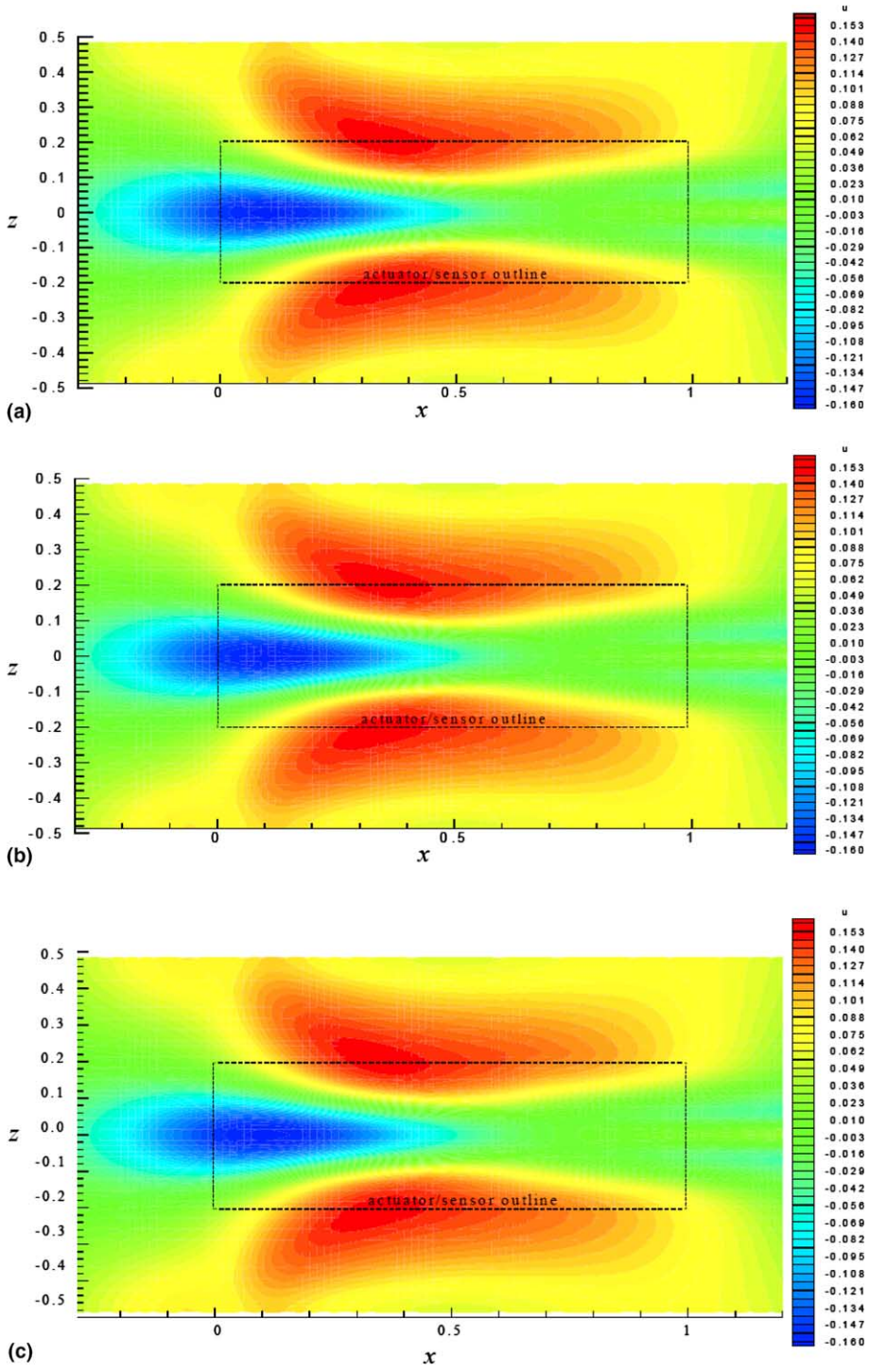

Fig. 13. Contours of u' at $y^+ = 12$. Uncontrolled streak core 10% along actuator. (a) No flow control; (b) flow control subroutine coupled to the new actuator design; (c) flow control subroutine coupled to the traditional actuator design.

strong positive fluctuations in the flow is consistent with the control strategy of accelerating the artificial streaks up to but not exceeding the local mean streamwise velocity. This strongly indicates the ability of the new actuator to focus the Lorentz forces on the designated target flow structure and to avoid introducing any superfluous Lorentz forces into the flow. The traditional actuator, by contrast, has not demonstrated nearly the same degree of focus. The artificial high speed streaks at $y^+ = 12$ have responded strongly to the large near wall ($y^+ < 5$) Lorentz forces beneath.

As the artificial low speed streak leaves through the downstream boundary of the actuator, located at $x = 1$, there is, however, some evidence of a slight over

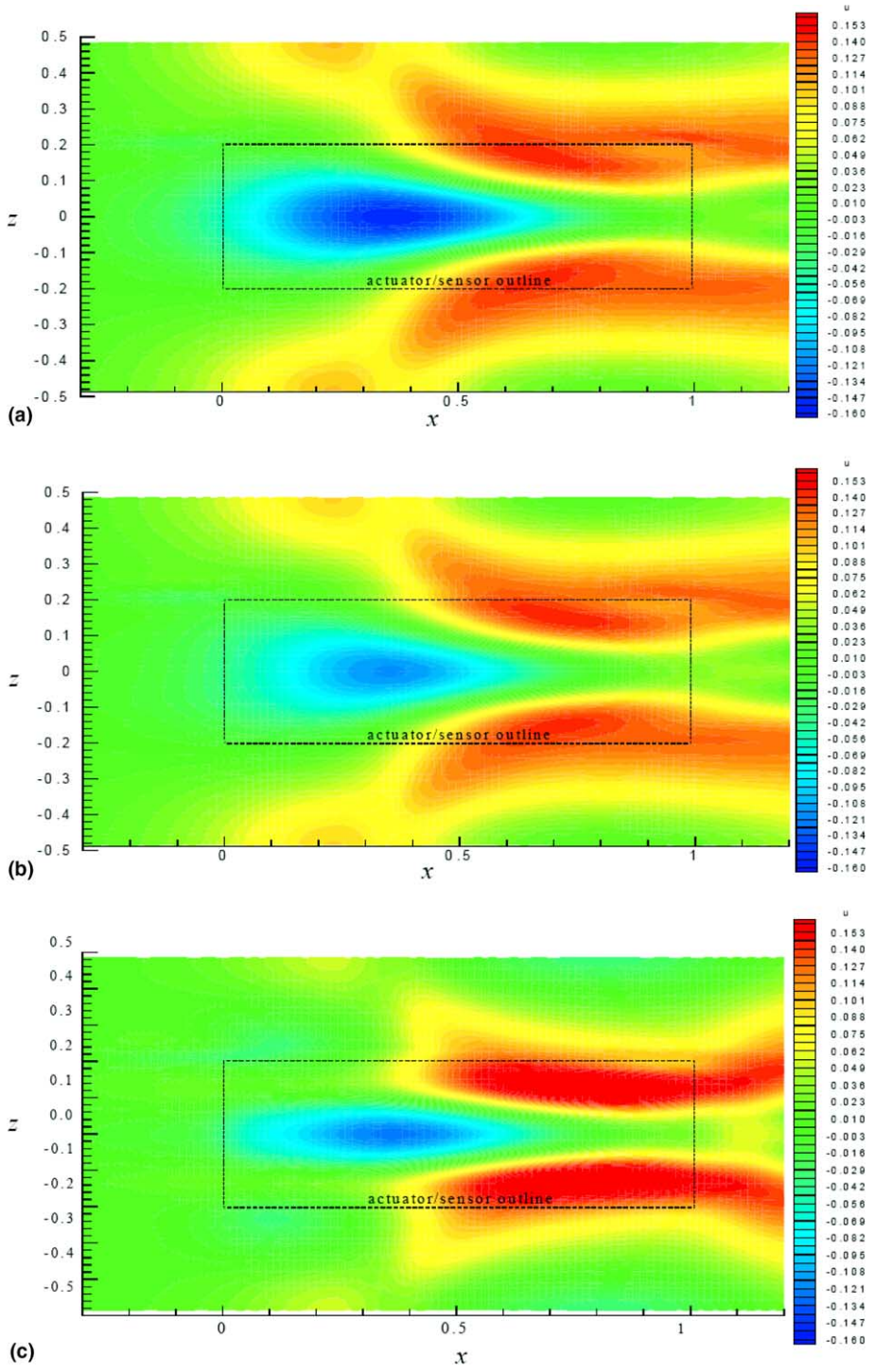

Fig. 14. Contours of u' at $y^+ = 12$. Uncontrolled streak core 35% along actuator. (a) No flow control; (b) flow control subroutine coupled to the new actuator design; (c) flow control subroutine coupled to the traditional actuator design.

forcing by the new actuator as indicated by the very light central region shown in Fig. 16b. This is not of great concern since the positive fluctuation is only about 7% of the local mean velocity and is quite localized extending streamwise for about 30% of the actuator length and spanwise for 25% of the actuator width. By contrast inspection of Fig. 16c reveals that the traditional actuator has induced a significant degree of over control as indicated by the large regions of very light and dark contours.

Examining the flow region above $y^+ = 12$ it can be seen that the new actuator design has successfully accelerated the majority of the artificial low speed streak back to the local mean streamwise velocity by the time

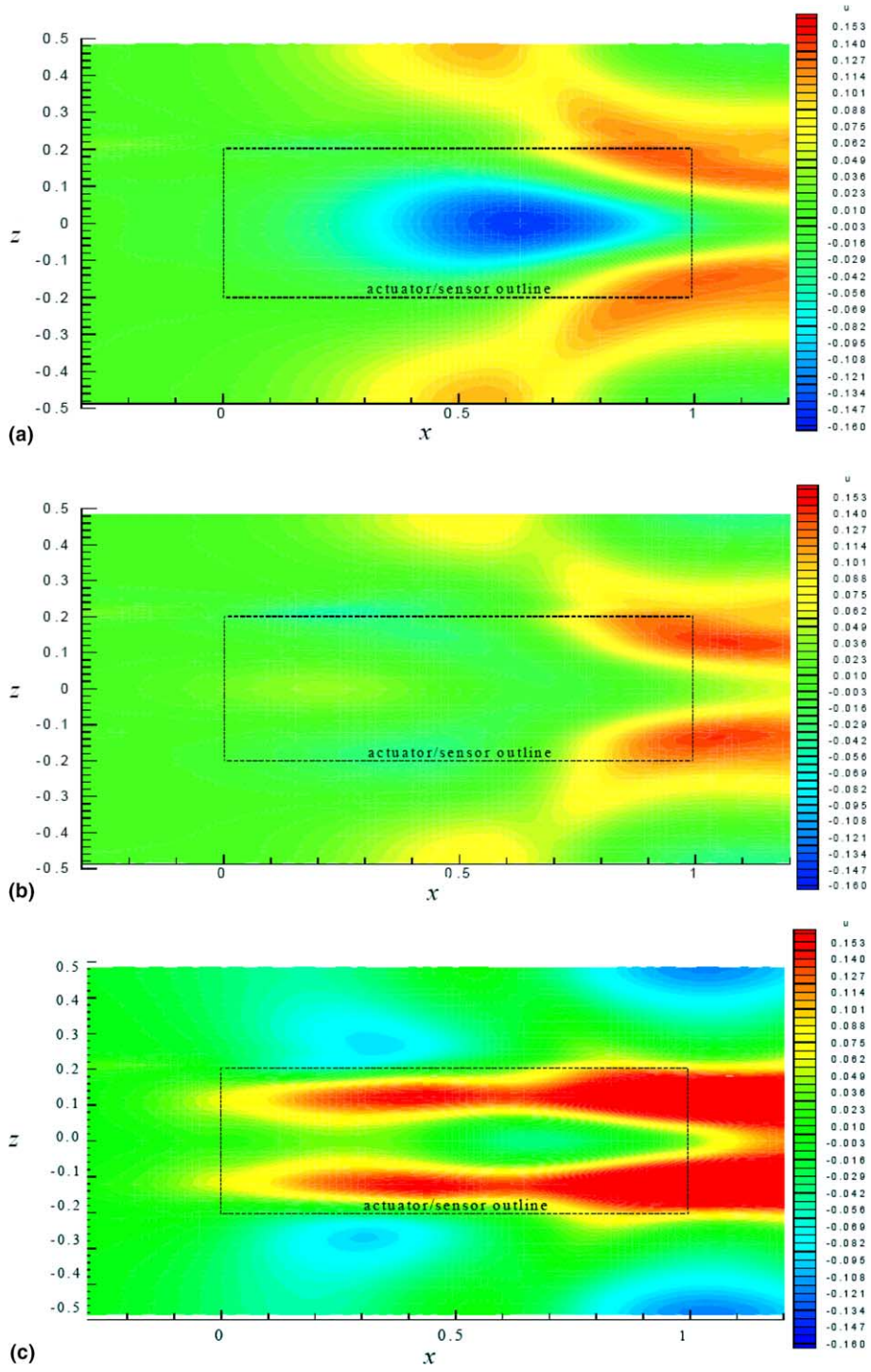

Fig. 15. Contours of u' at $y^+ = 12$. Uncontrolled streak core 65% along actuator. (a) No flow control; (b) flow control subroutine coupled to the new actuator design; (c) flow control subroutine coupled to the traditional actuator design.

the streak passes through the downstream boundary of the actuator at $x = 1.0$. This may be seen in Fig. 20b. In doing so we can confirm that the new actuator has been designed with a sufficient level of penetration into the flow to ensure that the bulk of the artificial low speed streak has been effectively targeted. The same can not be said for the traditional actuator design. In fact it may be seen in Figs. 18c, 19c and 20c that whilst the traditional actuator design has accelerated the flow at $y^+ = 12$, also see Figs. 13c, 14c, 15c and 16c, it has actually *decelerated* the portion of the low speed streak located above $y^+ = 12$. This is totally against the intended control

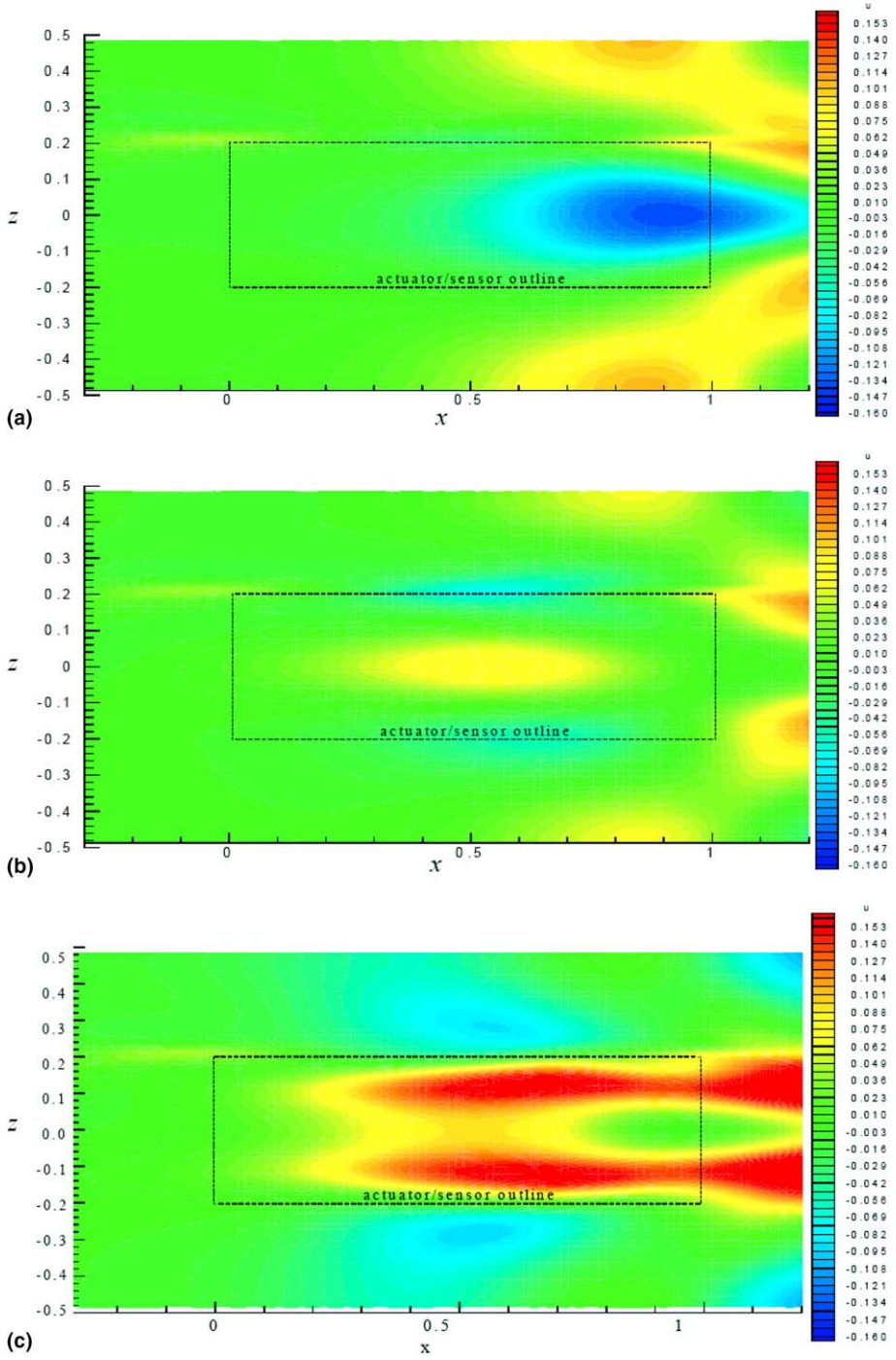

Fig. 16. Contours of u' at $y^+ = 12$. Uncontrolled streak core 90% along actuator. (a) No flow control; (b) flow control subroutine coupled to the new actuator design; (c) flow control subroutine coupled to the traditional actuator design.

strategy since it will encourage the ejection-burst-sweep process to occur and hence increase the frictional drag and turbulence intensity at the wall.

An equally marked contrast between the performance of the traditional actuator design and the new actuator design may be seen in the region below $y^+ = 12$. The time sequence for the new actuator design, Figs. 17b, 18b, 19b, 20b, reveals that throughout the process of attenuating the artificial low speed streak the velocity fluctuations below $y^+ = 12$ have remained near zero. In other words while the new actuator has been able to exert the required level of control over the artificial low speed streaks located above $y^+ = 12$, this manipulation has been accomplished without disturbing the state of the flow in the region below $y^+ = 12$. The same can not be said for the traditional actuator design.

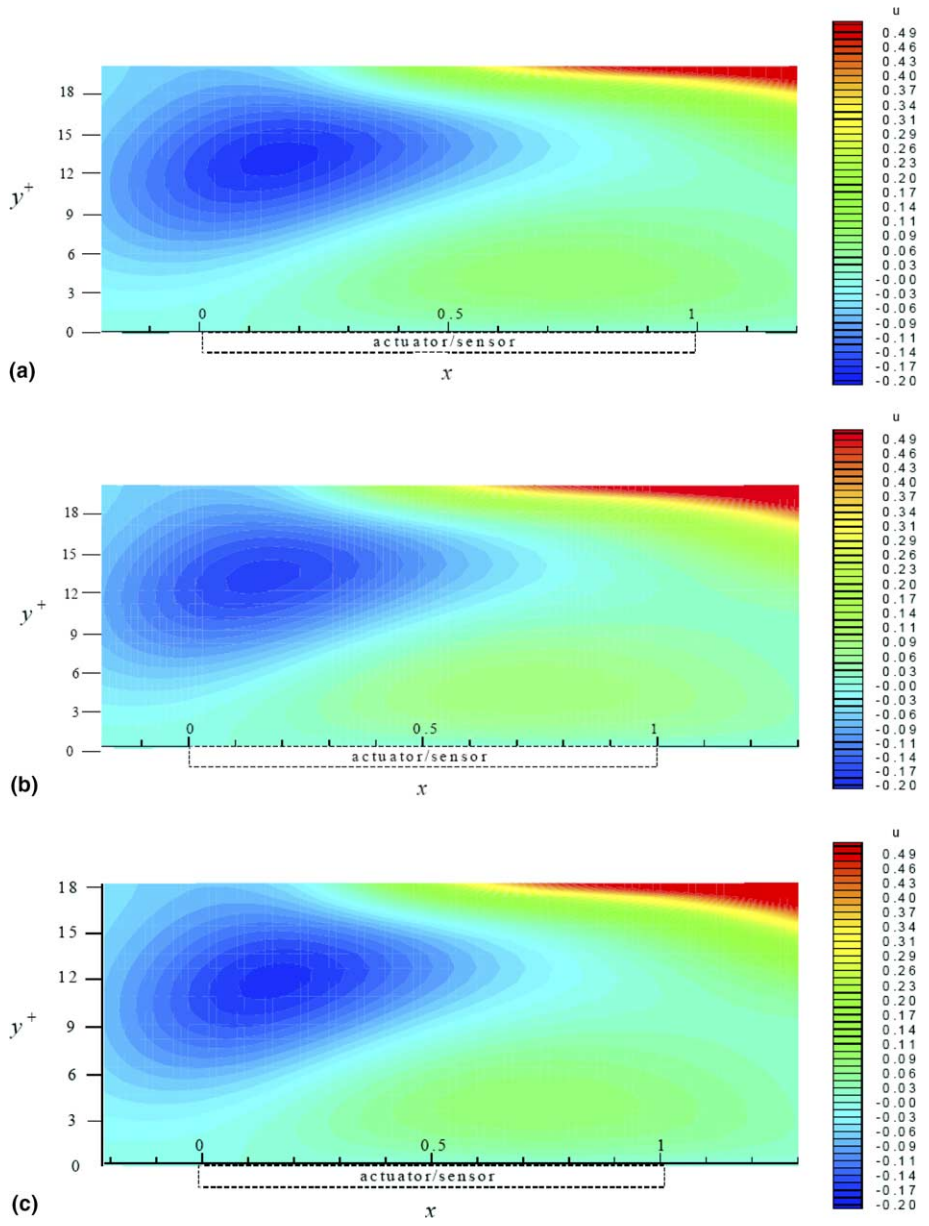

Fig. 17. Contours of u' in the spanwise symmetry plane. Uncontrolled streak core 15% along actuator. (a) No flow control; (b) flow control subroutine coupled to the new actuator design; (c) flow control subroutine coupled to the traditional actuator design.

The influence of the large near wall ($y^+ < 5$) Lorentz forces of the traditional actuator is particularly evident in Figs. 18c and 19c with the red contour regions indicating that the flow has had extremely high streamwise accelerations applied to it.

The immense significance of the new actuator's superior flow control in the $0 < y^+ < 12$ region is revealed by comparing the velocity gradients $\delta u/\delta y$ at the wall induced during the control of the artificial low speed streak. The gradients are computed using second order forward differencing and may be seen in Fig. 21. Note that in addition the gradients induced by the actuators, the velocity gradient of the mean velocity profile is also shown. This provides a reference for the case of perfect flow control since, ideally, the task of the actuator is to maintain a completely undisturbed flow at the wall. That is the controlling forces should perfectly cancel the presence of the low speed streaks. It may be seen from Fig. 21 that while the maximum velocity gradient induced by the new actuator design is only 1.4 times the mean value, the traditional actuator design, by contrast, has induced a large increase in the velocity gradient up to 3.5 times greater than the mean value.

Clearly then the ability of the new actuator design to focus the required level of control in the region above $y^+ = 12$ while at the same time avoiding the introduction of unnecessary Lorentz forces into the $0 < y^+ < 12$ region constitutes a significant advance in the performance

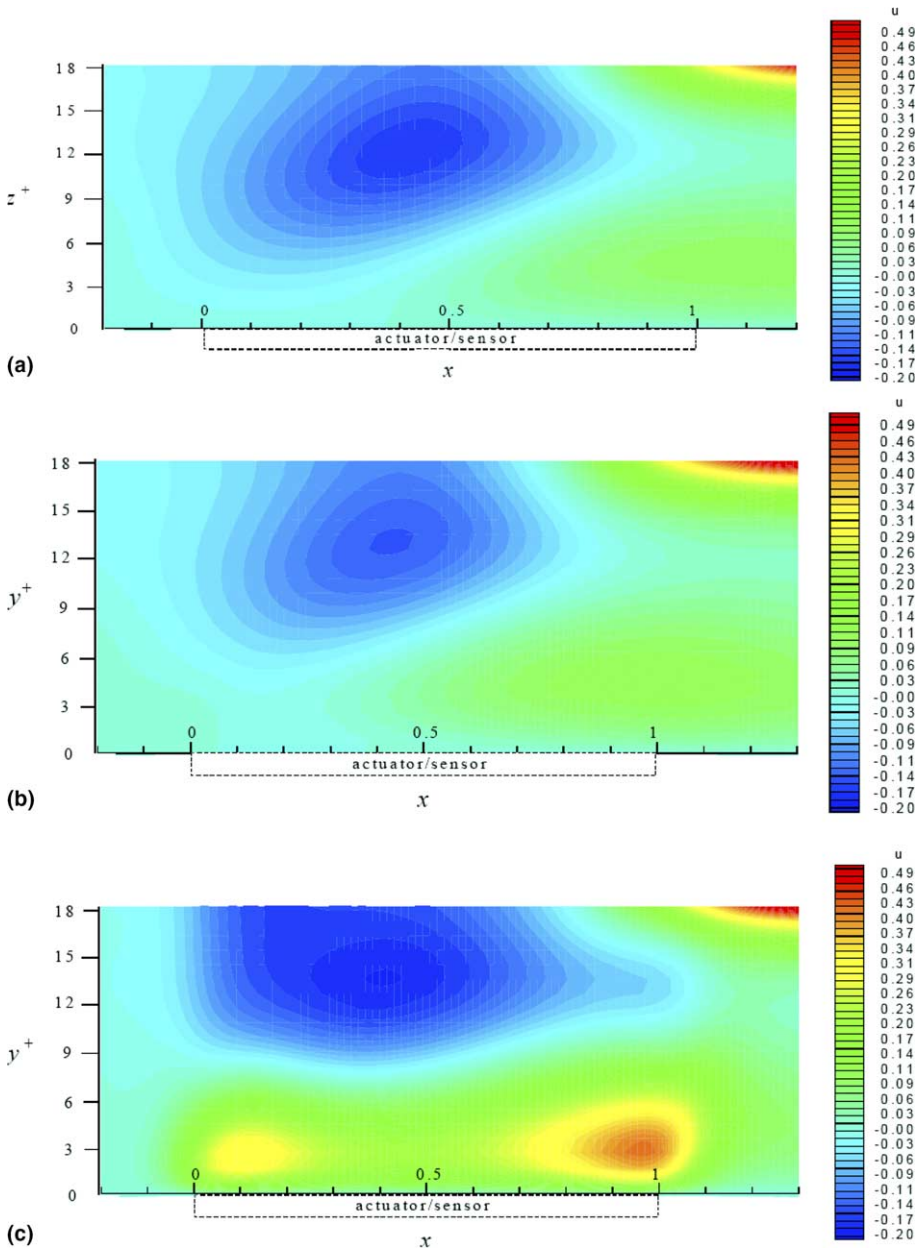

Fig. 18. Contours of u' in the spanwise symmetry plane. Uncontrolled streak core 40% along actuator. (a) No flow control; (b) flow control subroutine coupled to the new actuator design; (c) flow control subroutine coupled to the traditional actuator design.

of EMHD actuators. Although there have been no previous studies to provide confirmation, the poor performance of type EMHD actuators (Berger et al., 2000) is most likely due to the introduction of the large and unnecessary Lorentz forces into the $0 < y^+ < 12$ region. It would appear that, in the past, the reductions in turbulence intensity gained by accelerating the low speed streaks have been nullified by the increase turbulence intensity resulting from the poor spatial distribution of the Lorentz forces.

This is no longer the case. The new actuator design presented in this paper should allow the low speed streaks to be accelerated without causing a substantial increase in turbulence intensity. This advance in flow control performance has come about due to the unique parabolic profile of the new actuator's Lorentz force field. The profile has been developed to ensure that the Lorentz forces immediately adjacent to the wall ($y^+ < 5$) are minimized while the Lorentz forces in the $10 < y^+ < 15$ region, where the low speed streaks are located, are maximized.

In addition to the energy savings resulting from this more efficient spatial distribution of Lorentz forces, savings in energy are also made as a result of the more

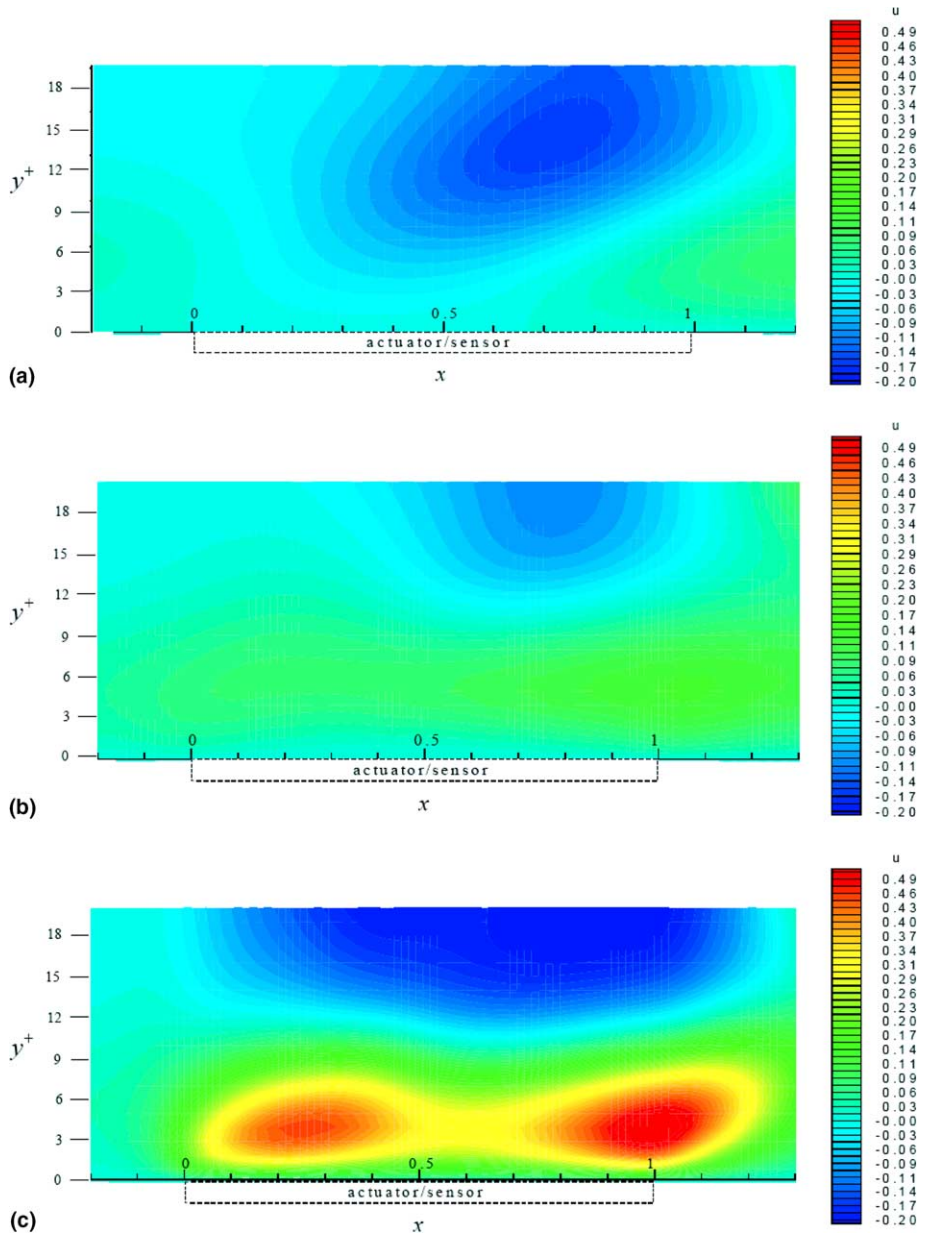

Fig. 19. Contours of u' in the spanwise symmetry plane. Uncontrolled streak core 70% along actuator. (a) No flow control; (b) flow control subroutine coupled to the new actuator design; (c) flow control subroutine coupled to the traditional actuator design.

efficient temporal distribution of Lorentz forces. By coupling the actuator to the *ideal sensor* and processing the sensor information through the flow control subroutine the total energy expenditure required to attenuate the sequence of artificial low speed streaks has been reduced to one eighth of the total energy which would be required if the actuator were permanently activated at its maximum non-dimensional strength of 1.0. This may be seen in Fig. 22 where the time dependency of the actuator power during control of the sequence of artificial low speed streaks is shown for both constant and variable power.

6. Conclusions

It has been demonstrated that one of the major reasons for the poor efficiency of EMHD flow control is that traditional EMHD actuators are incapable of focusing the Lorentz forces in the $10 < y^+ < 15$ region where the low speed streak structures, which are responsible for the high turbulence of boundary layer flows, are located. This deficiency is due to a strong decay in the Lorentz forces in the wallnormal direction. Therefore a new EMHD actuator design has been developed to provide a more efficient spatial distribution of the

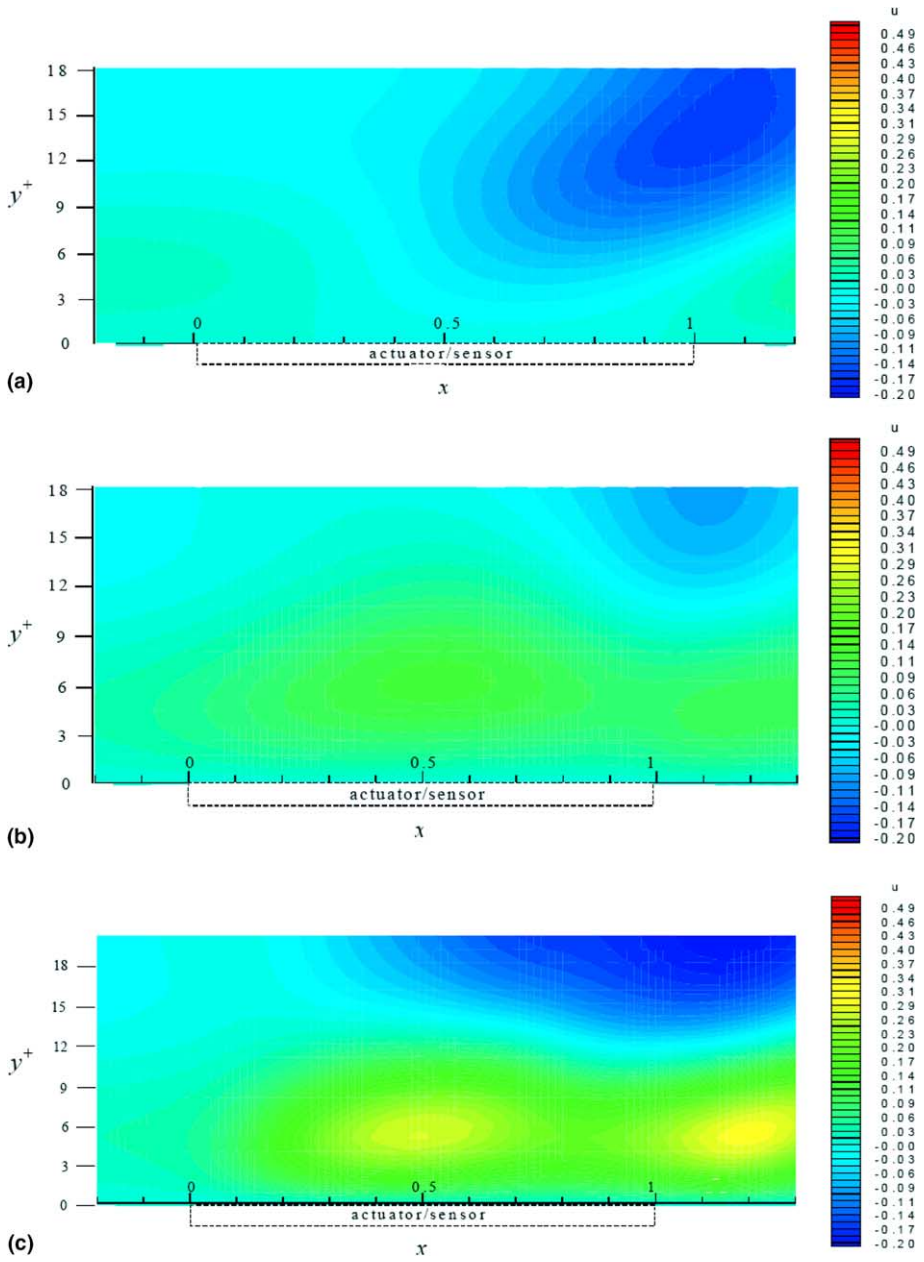

Fig. 20. Contours of u' in the spanwise symmetry plane. Uncontrolled streak core 100% along actuator. (a) No flow control; (b) flow control subroutine coupled to the new actuator design; (c) flow control subroutine coupled to the traditional actuator design.

electromagnetic forces so that control may be focused directly on the low speed streak structures.

The resulting new actuator has been shown to be a significantly superior design compared to traditional actuator designs in that it is capable of producing a Lorentz force field with a parabolic profile in the wallnormal direction rather than a decaying profile. As a result of the new design the maximum Lorentz force has been lifted from $y^+ = 0$ to approximately $y^+ = 5$ and the percentage contribution of the Lorentz forces in the $10 < y^+ < 15$ region increased from approximately 6% to 27%. It follows that the new actuator design has a much greater capacity to focus control on the low speed streaks.

In addition to the poor spatial distribution of the Lorentz forces the inefficiency of EMHD flow control can also be attributed to the poor temporal distribution of the forces. In previous EMHD flow control studies the Lorentz forces have been either constant or pulsed at arbitrary frequencies. Such an approach makes no allowance for the time dependency of the flow field to be controlled and invariably results in the Lorentz forces being applied to the flow at an inappropriate time and for an inappropriate strength and duration. Therefore the new

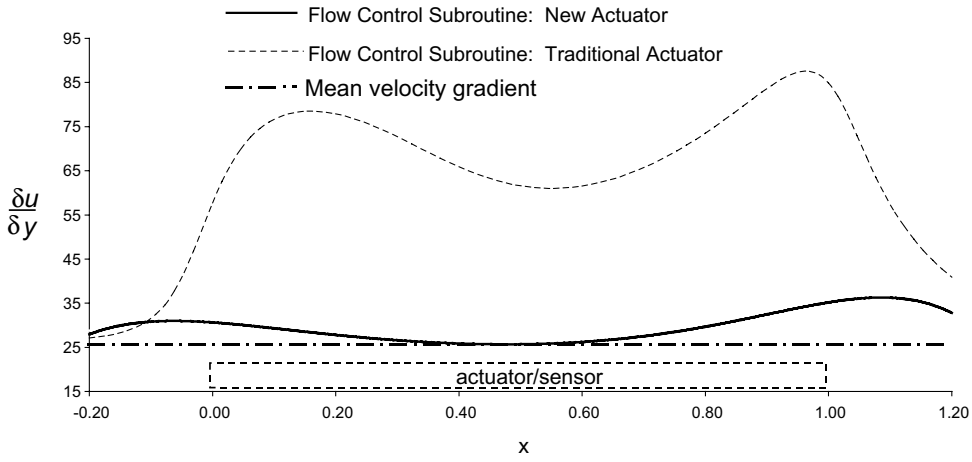

Fig. 21. Nondimensional velocity gradient at lower wall corresponding to uncontrolled streak core located 70% along actuator length.

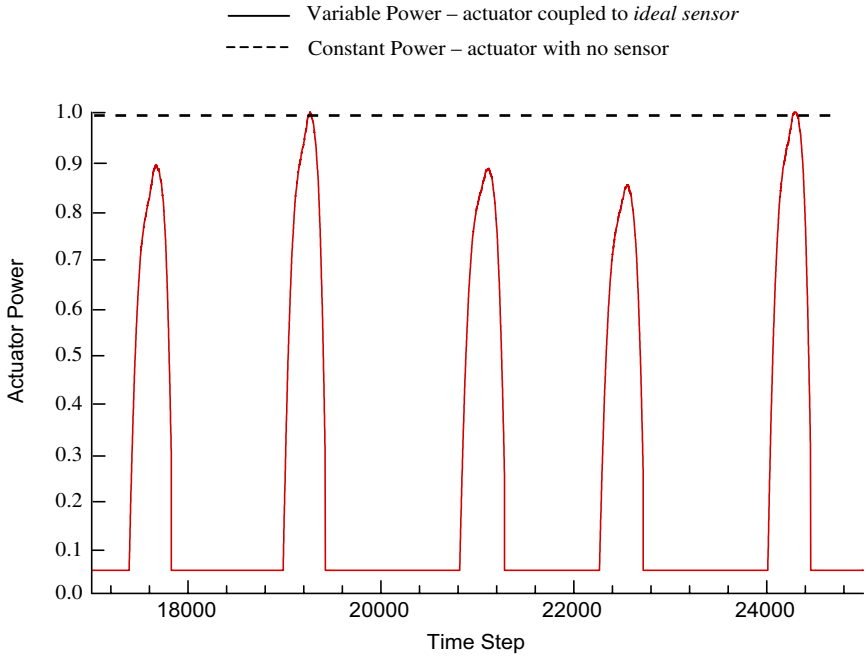

Fig. 22. Temporal distribution of non-dimensional actuator power.

actuator design has been coupled to an *ideal* sensor and a flow control subroutine developed to process the information from the *ideal* sensor so as to determine the appropriate actuating force. The appropriate actuating forces are predicted using a computational technique based on a linear superposition of velocity fields. This technique permits extremely fast and efficient solutions to be obtained for the time dependent Lorentz field.

The performance of the new actuator was assessed by generating a sequence of artificially induced low speed streaks which have been modeled to correspond with the Re 3300 turbulent channel flow investigated numerically by Kim et al. (1987). The artificial low speed streaks were passed over the actuator with the objective that they are detected and subsequently accelerated to the local mean streamwise velocity. The new actuator has been shown to successfully attenuate the artificial low speed streaks while inducing an increase in the instantaneous wall velocity gradient of only 40% of that induced by traditional EMHD actuators. By coupling the actuator to an ideal sensor the resulting total energy expenditure has been reduced to only 12% of that which would be required if the actuator were permanently activated at its maximum strength.

References

Berger, T.W., Kim, J., Lee, C., Lim, J., 2000. Turbulent boundary layer control utilizing the lorentz force. Physics of Fluids 12 (3), 631–649.

Crawford, C.H., Karniadakis, G.E., 1997. Reynolds stress analysis of EMHD controlled wall turbulence. Part 1. Streamwise Forcing. Physics of Fluids 9 (3), 788–806.

Du, Y., Crawford, C.H., Karniadakis, G.E., 1998. Lorentz Force Modeling in EMHD and Turbulence Control: DNS Studies, Centre for Fluid Mechanics #98-7, Brown University.

Du, Y., Karniadakis, G.E., 2000. Suppressing wall turbulence by means of a transverse traveling wave. Science 288, 1230–1234.

Henoch, C., Stace, J., 1995. Experimental investigation of a saltwater turbulent boundary layer modified by an applied streamwise magnetohydronamic body force. Physics of Fluids 7 (6), 1371–1383.

Kim, J., Moin, P., Moser, R., 1987. Turbulence Statistics in fully developed channel flow at low Reynolds Number. Journal of Fluid Mechanics 177, 133–166.

Posdziech, O., Grundmann, R., 2001. Electromagnetic control of Seawater flow around circular cylinders. Eur. J. Mech. B-Fluids 20, 255–274.

Spong, E., 2003. A Numerical Simulation of Adaptive Electromagnetic Flow Control, Ph.D. Thesis, The University of New South Wales, Sydney, Australia.